
CMS Physics Analysis Summary

Contact: cms-pag-conveners-susy@cern.ch

2017/03/21

Search for new physics in events with multileptons and jets in 35.9 fb^{-1} of proton-proton collision data at $\sqrt{s} = 13 \text{ TeV}$

The CMS Collaboration

Abstract

A search for new physics is carried out in events with at least 3 electrons or muons and jets. Results are based on the sample of 35.9 fb^{-1} of proton-proton collision data produced by the LHC at a center-of-mass energy of 13 TeV and collected by the CMS experiment. Events are classified according to the number of b jets, missing transverse momentum, hadronic transverse energy, and the invariant mass of opposite-charge, same-flavor dilepton pairs. No significant excess above the standard model background expectation is observed. The results are interpreted using simplified models of supersymmetry. Exclusion limits are set in the context of four different simplified supersymmetric models with pair production of gluino or 3rd generation squarks. In a model with gluino pair production, with subsequent decay into a top quark-antiquark pair and a neutralino, gluinos with masses smaller than 1610 GeV are excluded for light neutralinos. In a model with pair of bottom squarks production, the masses of sbottoms are excluded up to 840 GeV for light charginos.

1 Introduction

Many different beyond the standard model (BSM) theories predict processes leading to multilepton events. The background from standard model (SM) processes with this final state is small and dominated by the production of multiple bosons, which are well characterized both theoretically and experimentally in terms of cross section, branching ratios, and reconstruction of their various decay modes. This analysis is designed to have broad sensitivity to a variety of BSM models by examining the event yields as a function of several kinematic quantities.

This note describes the methods and results of a search for new physics in final states with three or more leptons accompanied by jets, using a proton-proton collisions at $\sqrt{s} = 13$ TeV, corresponding to an integrated luminosity of 35.9 fb^{-1} and recorded by the CMS detector at the CERN LHC during the year 2016. Results of this analysis will be interpreted in the context of supersymmetric (SUSY) models [1–9]. SUSY is a popular extension of the SM which predicts supersymmetric partners of the SM particles by introducing a new symmetry between bosons and fermions. Several SUSY models provide solutions to questions left open by the SM, such as the hierarchy problem and the nature of dark matter. More specifically, models in which R -parity [6] is conserved, and therefore SUSY particles are produced only in pairs, include dark matter candidates in the form of a stable and undetectable lightest supersymmetric particle (LSP). In the models considered in this note, the LSP is assumed to be the lightest neutralino (a mixture of the superpartners of neutral Higgs and electroweak bosons).

The reference models for this analysis are simplified model spectra (SMS) [10]. Examples for SUSY processes which can give rise to multilepton final states are shown in Figure 1. The models for this analysis feature the production of pairs of gluinos, superpartners of gluons, or squarks, superpartners of quarks, for a wide spectra of possible masses. These processes can result in several final state leptons through the decays of vector bosons. In addition to multiple leptons, these models predict events with multiple jets and missing transverse momentum, to which the predicted LSP contributes. The SUSY particles that are not directly included in the diagrams are assumed to be too heavy to be accessible at the LHC. Therefore, the free parameters in these models are usually the mass of the produced particle – here gluinos or squarks – and the mass of the LSP or chargino (a mixture of the superpartners of charged Higgs and electroweak bosons).

Typical processes within SUSY include gluino-pair production where each gluino decays to a $t\bar{t}$ pair and an LSP (Figure 1a), or to a pair of quarks and a neutralino or chargino ($\tilde{\chi}^\pm$). The latter would then decay into a Z or W boson, respectively, and the LSP (Figure 1b). Other models feature bottom squark (\tilde{b}) pair production, with cascade decays resulting in top quarks, W bosons and LSPs (Figure 1c) or pair production of the heavier of the two top squark (\tilde{t}_2) states, with subsequent decays to top quarks, Higgs and/or Z bosons, and LSPs (Figure 1d).

Similar searches have been carried out by ATLAS [11] and as well by CMS using the 8 TeV dataset [12, 13]. The searches continued with the data collected at the center-of-mass energy of 13 TeV. With 3.2 fb^{-1} of integrated luminosity collected by ATLAS [14], gluinos with masses up to 1200 GeV could be excluded in the model depicted in Figure 1a. A comparable search with 2.3 fb^{-1} of data collected with the CMS detector in 2015 was performed, gluinos with masses smaller than 1125 GeV could be excluded in a model with gluino pair production where the gluino decays to two top quarks and a neutralino [15].

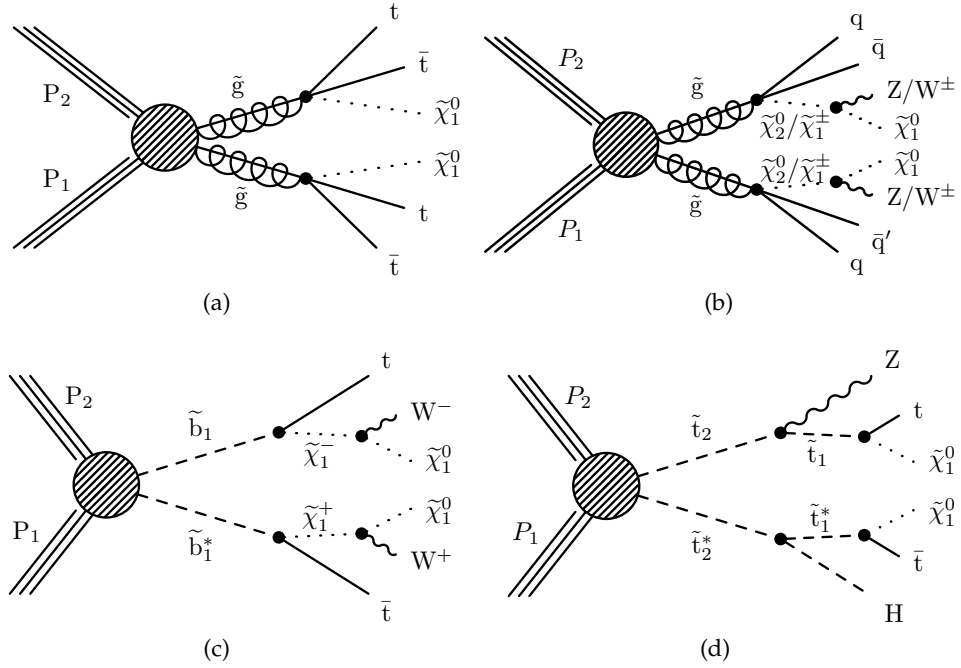


Figure 1: Diagrams for models involving gluino pair production leading to four top quarks (a), or four quarks and two vector bosons (b) in the final state, in both cases accompanied by two LSPs. Models of bottom and top squark pair production lead to two top quarks and, respectively, W bosons (c) or SM Higgs (H) or Z bosons (d).

2 The CMS detector

The CMS detector features a superconducting solenoid of 6 m internal diameter that creates a magnetic field of 3.8 T. Inside the magnet volume are a silicon pixel and strip tracker, an electromagnetic calorimeter (ECAL) made of lead tungstate crystals, and a hadron calorimeter (HCAL) made of brass and scintillator, each composed of a barrel and two endcap sections. Forward calorimeters provide additional pseudorapidity (η) coverage for the HCAL. Gas-ionization detectors in the steel flux-return yoke outside the solenoid are used to measure muons. The first level of the CMS trigger system, composed of specialized hardware processors, uses information from the calorimeters and muon detectors to select the most interesting events in a fixed time interval of less than 4 μ s. The high-level trigger (HLT) processor farm further decreases the event rate from approximately 100 kHz to around 1 kHz, before data storage. A more detailed description of the CMS detector, together with a definition of the coordinate system used and the relevant kinematic variables, can be found in Ref. [16].

3 Event selection and Monte Carlo simulation

Events of interest for this search are characterized by the presence of several physical objects, such as leptons or jets. The current section is aimed at providing a comprehensive list of their definitions within the context of this analysis.

Events are processed using the particle-flow (PF) algorithm [17, 18], which reconstructs and identifies each individual particle with an optimized combination of information from the various elements of the CMS detector. Jets are reconstructed from particle flow candidates [19], clustered with the anti- k_T algorithm and with a distance parameter of 0.4 [20]. Only jets with

transverse momentum (p_T) larger than 30 GeV and within the tracker acceptance $|\eta| < 2.4$ are considered. Additional criteria are applied to reject events containing noise and mismeasured jets. Jet energy scale (JES) corrections are applied to match jet energies measured in data and simulation.

A combined secondary vertex algorithm [21, 22] is used to assess the likelihood that a jet originates from a bottom quark. The tagging efficiency is typically 70% and a misidentification probability of 10% and 1% is for c- and light-flavor jets, respectively. The b jets with p_T greater than 25 GeV and within $|\eta| < 2.4$ are considered. The hadronic activity is defined as $H_T = \sum_{\text{jets}} p_T$, where all jets have $p_T > 30$ GeV.

Muon candidates are reconstructed combining the information from both the silicon tracker and the muon spectrometer in a global fit [23]. The identification is performed using the quality of the geometrical matching between the tracker and the muon system measurements. To ensure the candidates are within the fiducial volume of the detector, they are required to satisfy $|\eta| < 2.4$. The muon identification efficiency is at least 96%, with some variations depending on p_T and η .

Electron candidates are reconstructed using tracking and electromagnetic calorimeter information by combining ECAL superclusters and Gaussian Sum Filter tracks [24]. The electron identification is performed using a multivariate discriminant built with shower-shape variables, track-cluster matching variables, and track quality variables. The algorithm is optimized to select electrons from the decay of SM bosons with a 90% efficiency and to also efficiently reject candidates originating from jets. To reject electrons originating from photon conversion, electrons are required to have all possible hits in the innermost tracker layers and to be incompatible with any conversion-like secondary vertices. The selected electron candidates must have $|\eta| < 2.5$.

Both muon and electron candidates are required to have transverse impact parameter smaller than 0.5 mm w.r.t. the primary collision vertex in the event and a longitudinal impact parameter smaller than 1 mm. In addition, a selection on the 3D impact parameter significance, defined as the value of impact parameter divided by its uncertainty, is applied. This value has to be smaller than 4 for both electrons and muons.

In order to avoid double counting of objects, jets that have been matched geometrically to a lepton are removed from the list of jets in the event.

Additional information about the isolation of the lepton is necessary in order to discriminate between leptons originating from decays of heavy particles such as W and Z bosons (prompt leptons) and those produced in hadron decays or jets misidentified as leptons (nonprompt leptons). The lepton isolation criterion is constructed using three different variables. The relative isolation, I_{mini} , is defined as the ratio between the amount of measured energy in a cone around the lepton, with a p_T -dependent radius:

$$R = \frac{10 \text{ GeV}}{\min(\max(p_T(\ell), 50), 200)}, \Delta R \equiv \sqrt{(\Delta\eta)^2 + (\Delta\phi)^2}, \quad (1)$$

and the lepton p_T . The $\Delta\eta$ and $\Delta\phi$ are the difference in η and azimuthal angle (ϕ) between the considered lepton and the reconstructed object that contributes in at least one of the calorimeters. Requiring I_{mini} below a given threshold ensures that the lepton is locally isolated, even in boosted topologies.

The second variable is the ratio of the lepton p_T and the p_T of the jet geometrically matched to the lepton: $p_T^{\text{ratio}} = p_T(\ell) / p_T(\text{jet})$. In most of the cases, this is the jet containing the lepton. If no jet is found within a cone defined by $\Delta R < 0.4$, the ratio is set to 1. The use of p_T^{ratio} provides a way to identify nonprompt low- p_T leptons originating from low- p_T b-quarks which decay with larger opening angle than the one used in mini isolation.

The last variable used is p_T^{rel} , which is defined as the magnitude of the component of the lepton momentum perpendicular to the axis of the jet matched as described above. The jet axis is obtained by subtracting the momentum vector of the lepton from that of the jet. If no matched jet is found around the lepton, the variable is set to 0. This variable allows us to recover leptons from accidental overlap with jets in boosted topologies. For calculation of these both variables the jets with p_T greater than 5 GeV are considered.

Using those three variables, a lepton is considered isolated if the following condition is fulfilled:

$$I_{\text{mini}} < I_1 \wedge (p_T^{\text{ratio}} > I_2 \vee p_T^{\text{rel}} > I_3). \quad (2)$$

The $I_i, i = 1, 2, 3$ values depend of the flavor of the lepton: as the probability to misidentify a jet is higher for electrons than it is for muons, tighter isolation values are used for the former. For muons (electrons), the tight selection requirements are $I_1 = 0.16(0.12)$, $I_2 = 0.69(0.76)$, and $I_3 = 6.0(7.2)$ GeV. The loose lepton isolation is significantly relaxed: $I_{\text{mini}} < 0.4$ while the other requirements are dropped.

The missing transverse momentum E_T^{miss} is defined as the magnitude of \vec{p}_T^{miss} , the negative vector sum of all particle flow candidates reconstructed in an event [25].

Events used in this analysis are selected by trigger selections that target di- and multilepton events. One set of triggers requires that the two leptons meet loose isolation criteria and that the leading lepton has $p_T > 23$ GeV and the sub-leading lepton has $p_T > 8(12)$ GeV in the case of muons (electrons). The second set of triggers places no requirements on the isolation, has a lower p_T threshold for both leptons ($p_T > 8$ GeV), and also requires the H_T reconstructed in the trigger to be greater than 300 GeV.

The selection requires the presence of at least three well-identified leptons in the event. The leptons must satisfy p_T thresholds which are dependent on the lepton flavor and the hadronic activity in the event. For events with low hadronic activity ($H_T < 300$ GeV), the leading lepton must satisfy $p_T > 25$ GeV and subleading muons (electrons) must satisfy $p_T > 10(15)$ GeV respectively. In events with high hadronic activity ($H_T > 300$ GeV), the thresholds are relaxed to 10 (15) GeV for leading and subleading muon (electron). The third lepton must have $p_T > 10$ GeV all cases. Opposite-charge same-flavor lepton pairs are required to have an invariant mass ($m_{\ell\ell}$) greater than 12 GeV to reject Drell-Yan and quarkonia processes.

In order to estimate the contribution from SM processes with prompt leptons in the signal regions and to calculate the predicted yields from new physics models, Monte Carlo (MC) simulations are used. The `MADGRAPH5_AMC@NLO v2.2.2` [26] program is used for event generation at leading order (LO) or next-to-leading order (NLO) in perturbative QCD for all SM background processes, except diboson and single top production. For the latter, the `POWHEG v2` [27] generator is employed. Parton showering and hadronization are simulated using the `PYTHIA 8.205` generator [28] with the `CUETP8M1` tune [29]. The CMS detector response is determined using a `GEANT4`-based model [30]. The simulated samples include additional simultaneous interactions per bunch crossing (pileup), with distributions that are weighted to match the observed data.

Signal events for interpretation are generated with the `MADGRAPH5_AMC@NLO` program at LO precision, allowing up to two additional partons in the matrix element calculations. The SUSY particle decays, parton showering, and hadronization are simulated with `PYTHIA 8.205` [28]. The detector response for signal events is simulated using a CMS fast-simulation package [31] that is validated against the `GEANT4`-based model. All simulated events are processed with the same reconstruction procedure as data. Cross sections for SUSY signal processes, calculated at NLO with next-to-leading-log (NLL) resummation, are taken from the LHC SUSY Cross Sections Working Group [32–36].

4 Search strategy

A baseline selection is applied to the dataset containing events of interest: three or more electrons or muons, at least 2 jets ($N_{\text{jets}} \geq 2$), $E_{\text{T}}^{\text{miss}} \geq 50 \text{ GeV}$, and $m_{\ell\ell} \geq 12 \text{ GeV}$ for all opposite-charge, same-flavor lepton pairs. All these cuts are listed in Table 1. Two different regions are defined, based on whether an event contains an opposite-charge, same-flavor lepton pair with an invariant mass within a 15 GeV window around the Z mass or not. If such a lepton pair is found the event is categorized as on-Z and else as off-Z. In order to reject Drell-Yan events, the minimum $E_{\text{T}}^{\text{miss}}$ requirement is raised from 50 to 70 GeV in on-Z signal regions with low b jets multiplicity ($N_{\text{b jets}}$) and low H_{T} .

Table 1: Summary of all cuts used in baseline selection

Number of selected leptons	≥ 3
N_{jets}	≥ 2
$E_{\text{T}}^{\text{miss}}$	> 50 (70 in low $N_{\text{b jets}}$ and H_{T} category)
$m_{\ell\ell}$	> 12

Events are further categorized into signal regions, which are defined according to several event observables: $N_{\text{b jets}}$, H_{T} , $E_{\text{T}}^{\text{miss}}$, $m_{\ell\ell}$, and as well as the transverse mass reconstructed with a lepton and the missing transverse momentum vector:

$$M_{\text{T}} = \sqrt{2p_{\text{T}}E_{\text{T}}^{\text{miss}} \left[1 - \cos \left(\phi_{\ell} - \phi_{\vec{p}_{\text{T}}^{\text{miss}}} \right) \right]}. \quad (3)$$

If the event is flagged as on-Z, the M_{T} is calculated with the lepton that is not involved in the Z mass reconstruction, otherwise the lowest M_{T} among all leptons is considered.

The classification of selected events based on the number of b jets creates signal regions with high signal-to-noise ratio for events from different signal models. For example, the model with gluino pair production with further decay into 4 top quarks and 2 LSPs features several b jets, which would be categorized into signal regions that are almost free of WZ background owing to the b jet requirement. Including the 0 b jet signal regions keeps the analysis sensitive to signatures without b jets like the model with squark pair production. Additionally, a categorization in H_{T} and $E_{\text{T}}^{\text{miss}}$ is useful to distinguish between compressed and noncompressed SUSY spectra, i.e. models with small or large mass differences between the SUSY particles in the decay chain.

Table 2 shows the definition of the subdivision of the baseline selection into 16 off-Z and 16 on-Z signal regions (SR) respectively. The regions with $60 < H_{\text{T}} < 600$ and $50 < E_{\text{T}}^{\text{miss}} < 300$ are background dominated. In case of $N_{\text{b jets}} = 0$ and 1 and $60 < H_{\text{T}} < 400$ on-Z region the $E_{\text{T}}^{\text{miss}}$ lower bound is raised up to 70 GeV to completely suppress the contribution from the Drell-Yan process. Each such category is split depending on the number of b jets (0, 1 and 2) and the

value of H_T (greater and lower than 400 GeV) and E_T^{miss} (greater and lower than 150 GeV). Three additional SR with significant amount of H_T (SR 14,15) and E_T^{miss} (SR 16), respectively have been defined since various noncompressed SUSY model can yield events with very high E_T^{miss} or H_T . These regions are inclusive in the number of b jets. The split in M_T^{min} greater or lower than 120 GeV is done for 0 b-tag jet category and as well for 3 regions with high number of hadronic activity and E_T^{miss} . Motivated by the low expected yield of events with 3 or more b jets, one inclusive SR with $E_T^{\text{miss}} < 300$ and $H_T < 600$ has been defined for high b jet multiplicities ≥ 3 (SR 13).

Table 2: Summary of the definition of the signal regions. The minimum E_T^{miss} requirement is raised from 50 to 70 GeV only for on-Z SR1 and SR5. The dagger sign indicates signal regions that are further subdivided at $M_T^{\text{min}} = 120$ GeV. The search regions are mirrored in on- and off-Z region.

N_{jets}	$N_{\text{b jets}}$	H_T (GeV)	$50(70) \text{ GeV} \leq E_T^{\text{miss}} < 150 \text{ GeV}$	$150 \text{ GeV} \leq E_T^{\text{miss}} < 300 \text{ GeV}$	$E_T^{\text{miss}} \geq 300 \text{ GeV}$
≥ 2	0	60 – 400	SR1 †	SR2 †	SR16 †
		400 – 600	SR3 †	SR4 †	
	1	60 – 400	SR5	SR6	
		400 – 600	SR7	SR8	
	2	60 – 400	SR9	SR10	
		400 – 600	SR11	SR12	
	≥ 3	60 – 600	SR13		
	inclusive	≥ 600	SR14 †	SR15 †	

In order to provide a simplified version of the analysis for easier interpretation and reproducibility, a small set of aggregate signal regions has been defined, providing a compromise between simplicity and analysis sensitivity. The definition of the super signal regions is described in Table 3.

Table 3: Definition of super signal regions. A simpler classification is proposed for reinterpretations, depending on the presence of a Z candidate and the number of b jets, along with additional simultaneous requirements on M_T^{min} , E_T^{miss} and H_T .

$M_T^{\text{min}} \geq 120 \text{ GeV}$	on-Z	$N_{\text{b jets}} \leq 2$		$N_{\text{b jets}} \geq 3$	
		$H_T \geq 200 \text{ GeV}$	$E_T^{\text{miss}} \geq 250 \text{ GeV}$	$H_T \geq 60 \text{ GeV}$	$E_T^{\text{miss}} \geq 50 \text{ GeV}$
		No	SSR1		SSR2
Yes		SSR3		SSR4	

5 Background Estimation

Backgrounds for the multi-lepton final state can be divided in three categories:

- **Nonprompt or misidentified leptons** are leptons from heavy-flavor decays, misidentified hadrons, muons from light-meson decays in flight, or electrons from unidentified photon conversions. For this analysis $t\bar{t}$ events can enter the signal regions if nonprompt leptons are present in addition to the prompt leptons from the W decays. Top quark pair production is characterized by low H_T and low E_T^{miss} and therefore predominately populate signal regions 1 and 5, with 0 and 1 b jet respectively. Apart from $t\bar{t}$, Drell-Yan events can enter the baseline selection, however they are largely suppressed by the $E_T^{\text{miss}} > 50 \text{ GeV}$ selection and additional rejection is achieved by increasing the E_T^{miss} requirement to 70 GeV for on-Z regions with low H_T and low E_T^{miss} . Processes which yield only one prompt lepton in addition to nonprompt ones like W+jets and various single top channels are effectively suppressed by the three lepton requirement because of the low probability that two nonprompt leptons satisfy

the tight identification and isolation requirements, although this small contribution is nevertheless accounted for by our estimation method.

- **Diboson production** can yield multilepton final states with up to three prompt leptons for $WZ(\gamma^*)$ and up to four prompt leptons for $ZZ(\gamma^*)$ production (for simplicity referred to as WZ and ZZ respectively), rendering these processes irreducible backgrounds for this analysis. Especially in signal regions without b jets, WZ production has a sizable contribution in on- Z events.
- **Other rare SM processes** that can yield three or more leptons are $t\bar{t}W$, $t\bar{t}Z$, and tri-boson production VVV where $V = W, Z$. We also include the contribution from the SM Higgs boson produced in association with a vector boson or a pair of top quarks in this category of backgrounds, as well as processes that produce additional leptons from internal conversions, which are events that contain a virtual photon that decays to leptons. The internal conversion background components, $X+\gamma$, are heavily suppressed by the $E_T^{\text{miss}} > 50 \text{ GeV}$ and $N_{\text{jets}} \geq 2$ requirements. The contribution from these processes is estimated from MC simulation.

The background contribution from nonprompt and misidentified leptons is estimated using the tight-to-loose ratio method. In this method, the yield in an application region, populated by events that contain at least one lepton which fails the full set of tight identification and isolation requirements but satisfies the loose requirements, is weighted by $f/(1-f)$, where the tight-to-loose ratio f is the probability that a loosely identified lepton also satisfies the full set of requirements. This ratio is measured as a function of lepton p_T and η in a control sample of multijet events that is enriched in nonprompt leptons (measurement region): exactly one lepton satisfying the loose object selection is required in the event, and one recoiling jet with $\Delta R(\text{jet}, \ell) > 1.0$ and $p_T > 30 \text{ GeV}$. To suppress the contribution from W and Z bosons decaying to prompt leptons, we additionally require E_T^{miss} and M_T to be both below 20 GeV. The remaining contribution from these electroweak processes within the measurement region is subtracted using estimates from MC simulation.

In order to reduce the dependence of the tight-to-loose ratio on the flavor composition of the jets which the nonprompt leptons originate from, it's parameterized as a function of a variable that correlates more strongly with the mother parton p_T than with the lepton p_T . This variable is calculated by correcting the lepton p_T as a function of the energy in the isolation cone around it. This definition leaves the p_T of the leptons satisfying the isolation cut unchanged and modifies the p_T of those failing the cut so that it is a better proxy for the mother parton p_T and results in a smaller variation as a function of the mother parton p_T . The flavor dependence, which is much more important for the case of electrons, is also reduced by adjusting the loose object selection to obtain similar ratios for nonprompt electrons that originate from both light- and heavy-flavor jets. As a result, the tight-to-loose ratio measured in a multijet sample provides a good description of nonprompt background originating from $t\bar{t}$ events.

The tight-to-loose ratio method for estimating the nonprompt background is validated both in a closure test in simulation and in a data control region exclusive to our baseline selection with minimal signal contamination. This region is defined by the requirement of three leptons that satisfy the nominal identification, isolation and p_T selection, one or two jets, $30 < E_T^{\text{miss}} < 50 \text{ GeV}$, and no on- Z dilepton pair. With these cuts a purity in $t\bar{t}$ of 80% can be achieved. We find an agreement of the order of 20 – 30% between the predicted and observed yields in this control region.

The WZ process is one of the main backgrounds in the regions with 0 b jets, while $t\bar{t}Z$ gives a significant contribution in categories enriched in b jets. The estimates for these processes are

taken from simulation, but the normalization is obtained from a simultaneous fit using two control regions, designed so that each is highly enriched in one of the processes. The WZ control region is defined by the requirement of three leptons satisfying the nominal identification and isolation selections. Two leptons have to form an opposite charge, same flavor pair with $|m_{\ell\ell} - m_Z| < 15$ GeV, the number of jets and b jets has to be ≤ 1 and 0, respectively. The E_T^{miss} has to be in the range $30 \text{ GeV} < E_T^{\text{miss}} < 100 \text{ GeV}$, and the M_T is required to be at least 50 GeV to suppress contamination from the Drell-Yan process. The purity of the WZ control region is 80%. The orthogonal control region for $t\bar{t}Z$ is defined with similar as for WZ, except for a strict requirement on number of jets, requirements: three leptons satisfying the nominal identification and isolation selection, two leptons that form an opposite charge, same flavor pair with $|m_{\ell\ell} - m_Z| < 15$ GeV, at least 3 jets, and $30 \text{ GeV} < E_T^{\text{miss}} < 50 \text{ GeV}$. Events are classified by the number of b jets, and three bins are formed: the 0 b jet category, dominated in WZ and $t\bar{t}$ process, and 1 and the ≥ 2 b jet categories that are dominated by $t\bar{t}Z$. The overall purity in $t\bar{t}Z$ is 20%, increased to 50% in the bins with at least one b jet. These three bins and the WZ control region are used in a simultaneous fit to obtain the scale factors for the normalization of the simulated samples. For the WZ process the obtained scale factor is compatible with unity, 1.01 ± 0.07 , and no correction is applied to the simulation, while for the $t\bar{t}Z$ the obtained is found to be 1.14 ± 0.28 . Therefore the yields from MC $t\bar{t}Z$ sample obtained in baseline region is reweighted by a factor 1.15.

6 Systematic Uncertainties

The different uncertainties are categorized as experimental, as those related to the jet-energy scale or the b-tagging efficiency; theoretical, such as the uncertainties on the considered cross sections; statistical, related to the observed yield in control regions in data and the limited sample size of simulations; and uncertainties on the applied data-driven methods. These uncertainties and their effect on the predicted yields are described below and summarized in Table 4.

Table 4: Systematic uncertainties and their effect on the event yields of each affected process.

source	effect on yield
luminosity	2.6%
jet energy scale	1 – 10%
b-tag efficiency	1 – 10%
pileup	1 – 5%
lepton efficiencies	9%
HLT efficiencies	3%
lepton eff. FastSim	6%
nonprompt application region stat.	10 – 100%
nonprompt extrapolation	30%
WZ CR normalization	10%
$t\bar{t}Z$ CR normalization	25%
Limited size of simulated samples	1 – 100%
Modelling of unclustered energy	1-20%
ISR modeling	1-10%
QCD scales cross-section ($t\bar{t}W, t\bar{t}H$)	11 – 13%
QCD scales acceptance ($t\bar{t}W, t\bar{t}Z, t\bar{t}H$, signal)	1 - 18%
PDFs ($t\bar{t}W, t\bar{t}Z, t\bar{t}H$)	2 – 3%
other rare bkgs.	50%

One of the major experimental sources of uncertainty is the knowledge of the jet energy scale (JES). This uncertainty affects all simulated background and signal events. For the dataset used in this analysis, the uncertainties on the jet energy scale vary from 1% to 8%, depending of the transverse momentum and pseudorapidity of the jet. The impact of these uncertainties is assessed by shifting the jet energy correction factors for each jet up and down by 1σ and recalculating all kinematic quantities. The JES corrections are propagated to the E_T^{miss} as well. The propagation of the variation of the JES results in a variation of 1–10% in the event yields.

A similar approach is used for the uncertainties associated with the corrections for the b-tagging efficiencies for light and bottom flavor jets, which are parametrized as a function of p_T and η . The variation of the scale factor correcting for differences between data and simulation is at maximum of the order of 10% per jet, and leads to an overall effect in the range of 1–10% depending on the signal region and on the topology of the event.

Lepton identification and isolation scale factors have been measured as function of lepton p_T and η . They are applied to correct for residual differences in lepton selection efficiencies between data and simulation. The corresponding uncertainties are estimated to be about 3% per lepton for both flavors. Assuming correlation between the corrections of the different lepton a flat uncertainty of 9% is taken into account. The uncertainty related to the HLT trigger efficiency amounts to 3%.

The sources of uncertainties listed above have also been studied for the signal samples and their impact on the signal event yields has been estimated following the same procedures.

Theoretical uncertainties include the uncertainty on the QCD renormalization (μ_R) and factorization scales (μ_F), and on the knowledge of the parton density functions (PDF). The uncertainties are considered for several electroweak processes, namely $t\bar{t}H$, $t\bar{t}Z$, and $t\bar{t}H$, which are dominant backgrounds in some signal regions. Both the changes in acceptance and cross sections related to those effects are taken into account.

For the study of the renormalization and factorization uncertainties, variations up and down by a factor of two with respect to the nominal values of μ_F and μ_R are considered. The maximum difference in the yields with respect to the nominal case is observed when both scales are varied up and down simultaneously. The effect on the overall cross section is found to be $\sim 13\%$ for $t\bar{t}W$ and $\sim 11\%$ for $t\bar{t}H$. An additional, uncorrelated uncertainty on the acceptance corresponding to different signal regions is included. This effect is found to vary between 3% and 18% depending on the search region and process.

The uncertainty related to the PDF is estimated from the 100 NNPDF 3.0 replicas, computing the deviation with respect to the nominal yields for each of them, and for each signal region (the cross section and acceptance effect are considered together) [37]. The root mean square of the variations is taken as the value of the systematic uncertainty. Since no significant differences between signal regions have been found, a flat uncertainty of 3% (2%) is considered for $t\bar{t}W$ ($t\bar{t}Z, t\bar{t}H$). This value also includes the effect on $\alpha_S(M_Z)$, which is added in quadrature.

For the $t\bar{t}H$ process, the same Q^2 and PDF related uncertainties as estimated for $t\bar{t}Z$ are considered. A conservative uncertainty of 50% is assigned to the remaining rare processes.

For signal samples additional uncertainties for initial state radiation are taken into account. The modelling of initial state radiation (ISR) by the version of the MadGraph generator used for signal events was tested in a selection of $t\bar{t}$ events in the dilepton final state. The corresponding corrections range from 0.92 to 0.51, depending on the jet multiplicity. To improve on the MadGraph modeling of the multiplicity of additional jets from initial state radiation (ISR),

SUSY simulated events are reweighted based on the number of ISR jets (N_J^{ISR}) so as to make the jet multiplicity agree with data. For signal samples, half of the effect of the ISR correction are assigned as a systematic uncertainty. An uncertainty on potential differences of the modeling of E_T^{miss} in data and the fast simulation of the CMS detector is evaluated by comparing the reconstructed E_T^{miss} with the E_T^{miss} obtained using generator-truth information. This uncertainty ranges up to 20%.

The limited size of the generated Monte Carlo samples represents an additional source of uncertainty. For the backgrounds that are estimated from simulation, like $t\bar{t}W$, $t\bar{t}Z$ and $t\bar{t}H$, as well as for all the signal processes, uncertainty is computed from the number of Monte-Carlo events entering the signal regions and varies strongly across SRs.

For the nonprompt and misidentified lepton background, several systematic uncertainties are considered. The statistical uncertainty from the application region which is used to estimate this background contribution ranges from 10% to 100%. The regions where these uncertainties are large are generally regions where the overall contribution of this background is small. The uncertainty on electroweak subtraction is derived on the subtraction of prompt backgrounds in the measurement region. In the case where no events are observed in the application region, the upper limit of the background expectation is derived by multiplication of the most likely tight-to-loose ratio value by a Poisson fluctuation.

The systematic uncertainty related to the extrapolation from the control regions to the signal regions for the nonprompt lepton background is estimated to be 30%. This value has been extracted from closure tests which are performed by applying the method described in Section 5 to simulated samples yielding nonprompt leptons.

From the simultaneous fit in the control regions, the uncertainty on the normalization of the WZ process is estimated to be 10%, while a value of 25% is determined for $t\bar{t}Z$.

7 Results

A comparison of expected background events and data in distributions of the three event observables used for signal region categorization – H_T , E_T^{miss} , and $N_{\text{b jets}}$ – as well as for the lepton p_T spectra, the lepton flavor composition, and the lepton multiplicity in the event is shown in Figure 2 (Figure 3), using all the events satisfying the off-Z (on-Z) search region selection criteria. Figure 4 graphically presents a summary of predicted background and observed event yields in the individual signal regions. The same data is also presented in Tables 5 and 6 for the off-Z and on-Z regions, respectively. Table 7 represents the yields in super signal regions.

The number of events observed in data are found to be consistent with predicted background yields in all 46 signal regions. No significant deviation has been found. Therefore the results of the search are interpreted by setting limits on gluino and neutralino masses, using the simplified models for gluino pair production with four top quarks or two vector bosons and jets in the final state, and on the masses of squarks and chargino in the models with bottom and top squark pair production. For each mass point, the observation, background predictions, and expected signal yields from all on-Z and off-Z search regions are combined to extract a cross section that can be excluded at a 95% confidence level (CL) using the CLs method[38, 39] in an asymptotic formulation[40]. Log-normal nuisance parameters are used to describe the uncertainties listed in Section 6. The limits are shown in Figure 5a for the four-top model, in Figure 5b for the $VV + \text{jets}$ model and in Figure 6 and 7 for 3rd generation squark pair production.

Compared to the previous search published by the CMS Collaboration [15], the current analysis

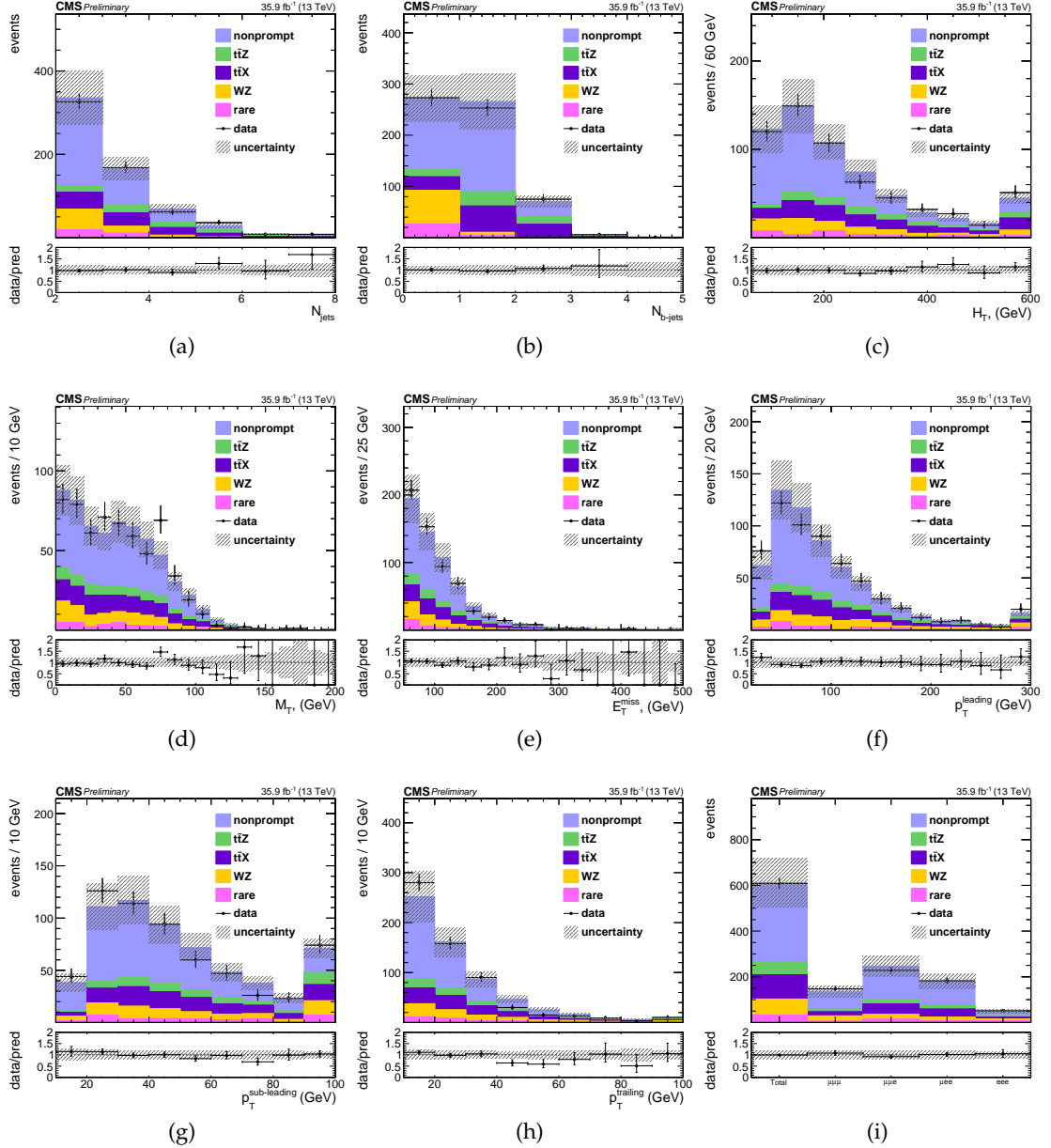


Figure 2: Background prediction and observation in key observables of the off-Z baseline selection: the number of (b) jets, H_T , M_T^{\min} , E_T^{miss} , the distributions of the lepton p_T spectra, the flavor composition of the leptons, and the event yields in each flavour category in the event are shown. The hatched area represents the statistical and systematic uncertainties on the prediction. The lower panels show the ratio of observation to prediction.

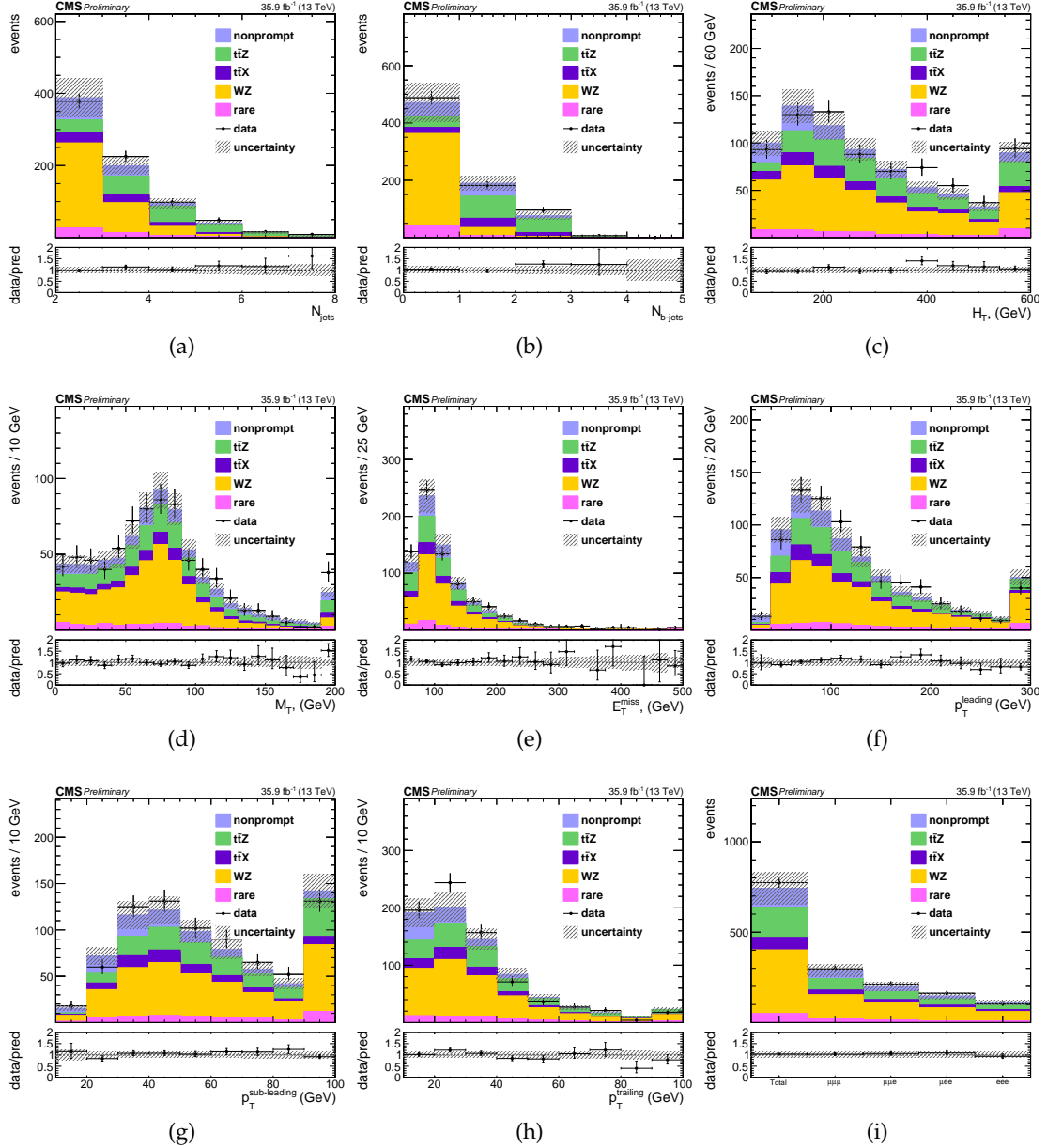


Figure 3: Background prediction and observation in key observables of the on-Z baseline selection: the number of (b) jets, H_T , M_T^{\min} , E_T^{miss} , the distributions of the lepton p_T spectra, the flavor composition of the leptons, and the event yields in each flavour category in the event are shown. The hatched area represents the statistical and systematic uncertainties on the prediction. The lower panels show the ratio of observation to prediction.

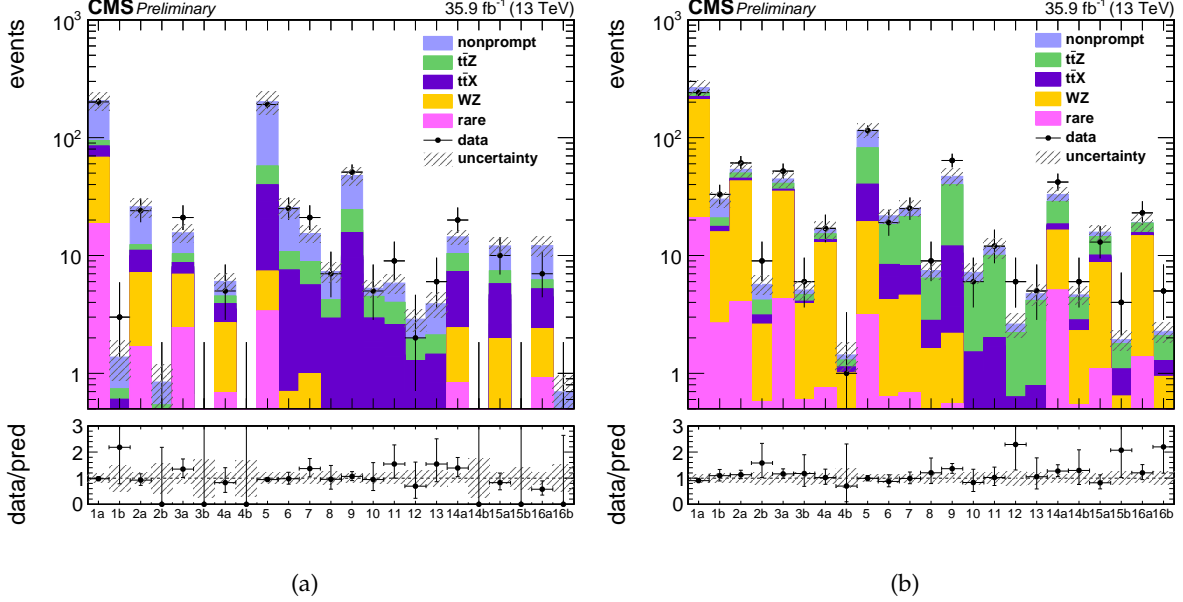


Figure 4: Background prediction and observation in the 23 off-Z signal regions and in the 23 on-Z signal regions. The hatched area represents the statistical and systematic uncertainties on the prediction. The lower panels show the ratio of observation to prediction.

Table 5: Observed and expected yields in the off-Z search regions with the 35.9 fb^{-1} of data. The uncertainties shown are statistical then systematic.

b-tags	H_T (GeV)	E_T^{miss} (GeV)	M_T (GeV)	Expected	Observed	SR
0 b-tags	60-400	50-150	< 120	$206 \pm 6 \pm 35$	201	SR1a
			≥ 120	$1.4 \pm 0.5 \pm 0.2$	3	SR1b
		150-300	< 120	$25.9 \pm 2.1 \pm 4.3$	24	SR2a
			≥ 120	$0.84 \pm 0.34 \pm 0.12$	0	SR2b
	400-600	50-150	< 120	$15.6 \pm 1.6 \pm 2.1$	21	SR3a
			≥ 120	$0.19 \pm 0.09 \pm 0.02$	0	SR3b
		150-300	< 120	$6.0 \pm 0.8 \pm 0.7$	5	SR4a
			≥ 120	$0.19 \pm 0.09 \pm 0.04$	0	SR4b
1 b-tags	60-400	50-150	inclusive	$202 \pm 6 \pm 44$	191	SR5
		150-300		$25.6 \pm 1.9 \pm 4.6$	25	SR6
	400-600	50-150		$15.4 \pm 1.3 \pm 2.2$	21	SR7
		150-300		$7.3 \pm 1 \pm 1.1$	7	SR8
2 b-tags	60-400	50-150	inclusive	$47.7 \pm 2.8 \pm 7.6$	51	SR9
		150-300		$5.3 \pm 0.5 \pm 0.6$	5	SR10
	400-600	50-150		$5.8 \pm 0.7 \pm 0.8$	9	SR11
		150-300		$2.9 \pm 0.5 \pm 0.4$	2	SR12
≥ 3 b-tags	60-600	50-300	inclusive	$3.9 \pm 0.7 \pm 0.6$	6	SR13
inclusive	≥ 600	50-150	< 120	$14.4 \pm 1.2 \pm 1.6$	20	SR14a
			≥ 120	$0.28 \pm 0.14 \pm 0.04$	0	SR14b
	≥ 60	≥ 300	< 120	$12.1 \pm 1.4 \pm 1.6$	10	SR15a
			≥ 120	$0.40 \pm 0.12 \pm 0.05$	0	SR15b
			< 120	$12.1 \pm 1.5 \pm 1.9$	7	SR16a
			≥ 120	$0.70 \pm 0.25 \pm 0.11$	0	SR16b

Table 6: Observed and expected yields in the on-Z search regions with the 35.9 fb^{-1} of data. The uncertainties shown are statistical then systematic.

b-tags	H_T (GeV)	E_T^{miss} (GeV)	M_T (GeV)	Expected	Observed	SR	
0 b-tags	60-400	50-150	< 120	$266 \pm 5 \pm 39$	241	SR1a	
			≥ 120	$30 \pm 2 \pm 4$	33	SR1b	
		150-300	< 120	$53.8 \pm 2.2 \pm 8$	61	SR2a	
			≥ 120	$5.69 \pm 0.76 \pm 0.69$	9	SR2b	
	400-600	50-150	< 120	$44.6 \pm 1.9 \pm 6.5$	52	SR3a	
			≥ 120	$5.1 \pm 0.6 \pm 0.7$	6	SR3b	
		150-300	< 120	$16.6 \pm 1.3 \pm 2.5$	17	SR4a	
			≥ 120	$1.43 \pm 0.33 \pm 0.2$	1	SR4b	
1 b-tags	60-400	50-150	inclusive	$115.70 \pm 3.50 \pm 15.23$	115	SR5	
				$21.7 \pm 1.2 \pm 2.8$	19	SR6	
		150-300		$25.2 \pm 1.2 \pm 3.6$	25	SR7	
				$7.5 \pm 0.8 \pm 1$	9	SR8	
	400-600	50-150		$47 \pm 1.6 \pm 7.4$	64	SR9	
				$7.2 \pm 0.8 \pm 1.2$	6	SR10	
		150-300		$11.7 \pm 1 \pm 2.1$	12	SR11	
				$2.6 \pm 0.4 \pm 0.4$	6	SR12	
≥ 3 b-tags	60-600	50-300	inclusive	$4.7 \pm 0.5 \pm 0.9$	5	SR13	
inclusive	≥ 600	50-150	< 120	$33 \pm 2 \pm 4$	42	SR14a	
			≥ 120	$4.6 \pm 0.6 \pm 0.6$	6	SR14b	
		150-300	< 120	$15.8 \pm 1.2 \pm 2$	13	SR15a	
			≥ 120	$1.9 \pm 0.3 \pm 0.2$	4	SR15b	
	≥ 60	≥ 300	< 120	$19.1 \pm 1.1 \pm 2.8$	23	SR16a	
			≥ 120	$2.28 \pm 0.35 \pm 0.26$	5	SR16b	

Table 7: Observed and expected yields in the super search regions with the 35.9 fb^{-1} of data. The uncertainties shown are statistical then systematic.

	fakes	$t\bar{t}Z$	ttX	WZ	rare	total	observed
SSR1	$0.63 \pm 0.38 \pm 0.19$	$0.14 \pm 0.06 \pm 0.03$	$0.23 \pm 0.04 \pm 0.05$	$0.01 \pm 0.01 \pm 0.01$	$0.12 \pm 0.06 \pm 0.05$	$1.1 \pm 0.4 \pm 0.2$	0
SSR2	$0.00 \pm 0.00^{+0.3}_{-0.0}$	$0.05 \pm 0.03 \pm 0.01$	$0.11 \pm 0.04 \pm 0.02$	$0.01 \pm 0.01 \pm 0.01$	$0.01 \pm 0.01 \pm 0.01$	$0.16 \pm 0.05^{+0.3}_{-0.02}$	0
SSR3	$0.46 \pm 0.37 \pm 0.14$	$1.27 \pm 0.18 \pm 0.31$	$0.50 \pm 0.07 \pm 0.08$	$1.03 \pm 0.28 \pm 0.21$	$0.40 \pm 0.09 \pm 0.14$	$3.7 \pm 0.5 \pm 0.4$	6
SSR4	$0.21^{+0.23}_{-0.21} \pm 0.06$	$0.54 \pm 0.10 \pm 0.13$	$0.17 \pm 0.03 \pm 0.02$	$0.01 \pm 0.01 \pm 0.01$	$0.01 \pm 0.01 \pm 0.01$	$0.92^{+0.26}_{-0.23} \pm 0.15$	2

improves the exclusion limits on gluino pair production models by approximately 400 GeV for the gluino mass and 250 GeV for the LSP in the four-top decay scenario, and by 200 GeV for both masses in the VV + jets final state.

8 Conclusions

A search for beyond the standard model physics in final states with ≥ 3 leptons, electrons or muons, using 35.9 fb^{-1} of data collected with the CMS detector in 2016 at $\sqrt{s} = 13 \text{ TeV}$ has been presented. The analysis makes use of control regions in data to estimate reducible backgrounds and to validate simulation for use in estimating irreducible background processes. To maximize

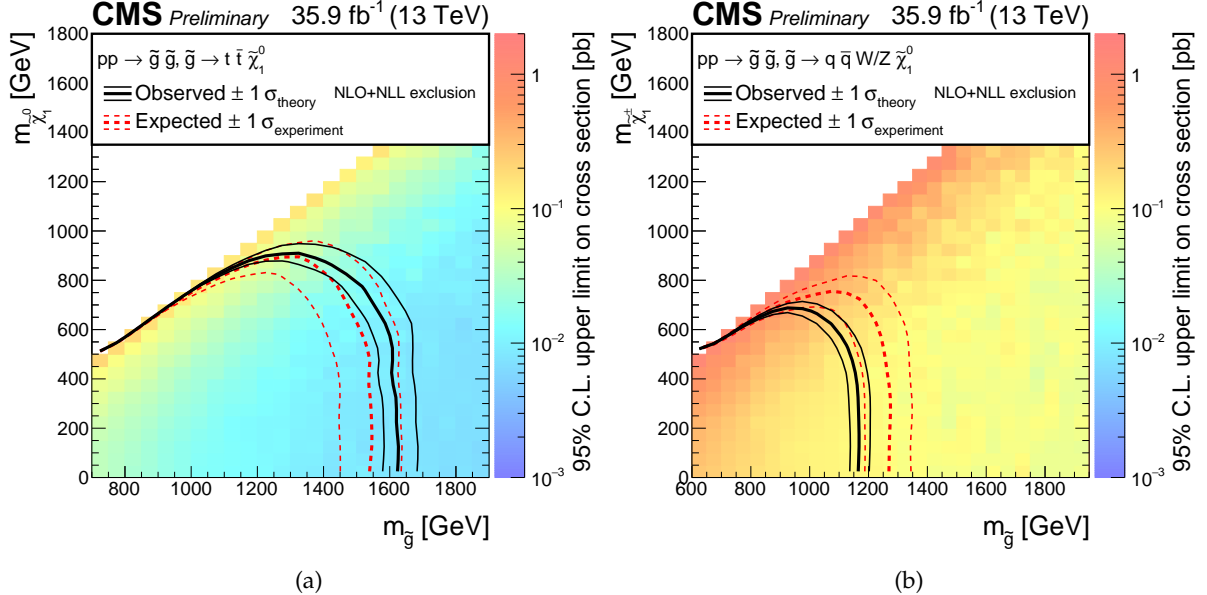


Figure 5: Excluded region at 95% confidence in the $m(\tilde{\chi}_1^0)$ versus $m(\tilde{g})$ plane for the simplified models of gluino pair production with four top quarks (a) and a VV + jets (b) in the final state. The excluded regions are to the left and below the observed and expected limit curves. The color scale indicates the excluded cross section at a given point in the mass plane.

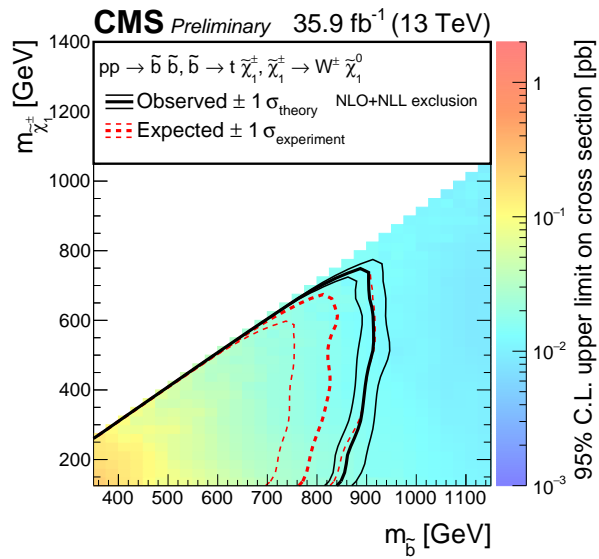


Figure 6: Excluded region at 95% confidence in the $m(\tilde{\chi}_1^0)$ versus $m(\tilde{b})$ plane for the simplified models of \tilde{b} pair production with two top quarks and two W boson + jets (b) in the final state. The excluded regions are to the left and below the observed and expected limit curves. The color scale indicates the excluded cross section at a given point in the mass plane.

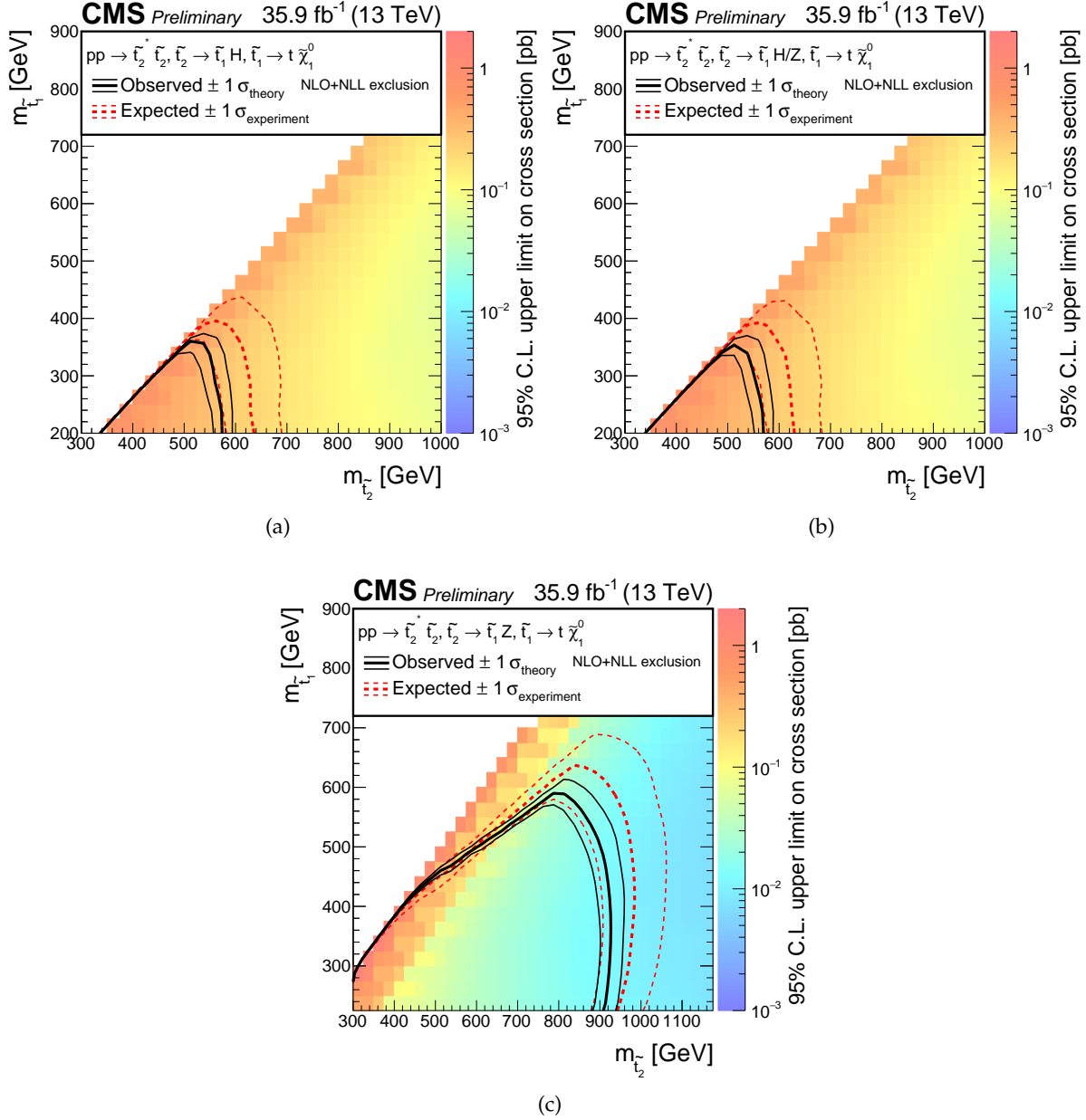


Figure 7: Excluded region at 95% confidence in the $m(\tilde{t}_2)$ versus $m(\tilde{t}_1)$ plane for the simplified models of \tilde{t}_2 pair production with 2 top quarks and two Z or H boson + jets (b) in the final state. Different branching ratio of the decay $\tilde{t}_2 \rightarrow \tilde{t}_1 Z$ are considered: 0% (a), 50% (b) and 100% (c). The excluded regions are to the left and below the observed and expected limit curves. The color scale indicates the excluded cross section at a given point in the mass plane.

sensitivity to a broad range of possible signal models, 46 exclusive signal regions have been investigated. No significant deviation from the expected standard model background has been observed.

In the absence of any observed excesses in the data, the result has been interpreted using a simplified gluino-pair production model that features cascade decays producing four top quarks in the final state. In this model, we exclude gluinos with a mass of up to 1610 GeV in the case of a massless LSP. The maximum excluded LSP mass is 900 GeV. In both masses, this represents an improvement of the order of 435 GeV and 250 GeV, respectively, compared to the exclusion limit set in a similar search based on 2.3 fb^{-1} collected with the CMS detector in 2015 [15].

For the simplified model with gluino-gluino production and light jets and two vector bosons in the final state, gluino masses up to 1160 GeV and neutralino masses up to 650 GeV can be excluded. The limit on gluino mass for a light neutralino extends the corresponding limit from the previous analysis by about 335 GeV and 150 GeV, respectively.

For simplified model for \tilde{b} pair production \tilde{b} masses up to 840 GeV is excluding in case of low mass of $\tilde{\chi}^\pm$, while $\tilde{\chi}^\pm$ masses are excluded up to 740 GeV, which are extending by 390 and 440 GeV for both sparticles.

And finally for top squarks pair production model with further decay into 2 top quarks and Higgs or Z boson, the \tilde{t}_2 masses are excluded up to 580, 570 and 910 GeV for the models with the $t_2 \rightarrow \tilde{t}_1 Z$ BR of 0%, 50% and 100% respectively, while \tilde{t}_1 masses are excluded up to 40, 10 and 300 GeV for the same branching ratios.

References

- [1] P. Ramond, "Dual theory for free fermions", *Phys. Rev. D* **3** (1971) 2415, doi:10.1103/PhysRevD.3.2415.
- [2] Yu. A. Golfand and E. P. Likhtman, "Extension of the algebra of Poincare group generators and violation of P invariance", *JETP Lett.* **13** (1971) 323. [Pisma Zh. Eksp. Teor. Fiz. **13** (1971) 452].
- [3] A. Neveu and J. H. Schwarz, "Factorizable dual model of pions", *Nucl. Phys. B* **31** (1971) 86, doi:10.1016/0550-3213(71)90448-2.
- [4] D. V. Volkov and V. P. Akulov, "Possible universal neutrino interaction", *JETP Lett.* **16** (1972) 438. [Pisma Zh. Eksp. Teor. Fiz. **16** (1972) 621].
- [5] J. Wess and B. Zumino, "A lagrangian model invariant under supergauge transformations", *Phys. Lett. B* **49** (1974) 52, doi:10.1016/0370-2693(74)90578-4.
- [6] J. Wess and B. Zumino, "Supergauge transformations in four-dimensions", *Nucl. Phys. B* **70** (1974) 39, doi:10.1016/0550-3213(74)90355-1.
- [7] P. Fayet, "Supergauge invariant extension of the Higgs mechanism and a model for the electron and its neutrino", *Nucl. Phys. B* **90** (1975) 104, doi:10.1016/0550-3213(75)90636-7.
- [8] H. P. Nilles, "Supersymmetry, supergravity and particle physics", *Phys. Rept.* **110** (1984) 1, doi:10.1016/0370-1573(84)90008-5.
- [9] S. P. Martin, "A supersymmetry primer", in *Perspectives on Supersymmetry II*, G. L. Kane, ed., p. 1. 2010. arXiv:hep-ph/9709356. Adv. Ser. Direct. High Energy Phys., vol. 21. doi:10.1142/9789814307505_0001.
- [10] D. Alves et al., "Simplified models for LHC new physics searches", *J. Phys. G* **39** (2012) 105005, doi:10.1088/0954-3899/39/10/105005, arXiv:1105.2838.
- [11] ATLAS Collaboration, "Search for supersymmetry at $\sqrt{s} = 8$ TeV in final states with jets and two same-sign leptons or three leptons with the ATLAS detector", *JHEP* **06** (2014) 035, doi:10.1007/JHEP06(2014)035, arXiv:1404.2500.
- [12] CMS Collaboration, "Search for anomalous production of events with three or more leptons in pp collisions at $\sqrt{s} = 8$ TeV", *Phys. Rev. D* **90** (2014) 032006, doi:10.1103/PhysRevD.90.032006, arXiv:1404.5801.
- [13] CMS Collaboration, "Searches for supersymmetry based on events with b jets and four W bosons in pp collisions at 8 TeV", *Phys. Lett. B* **745** (2015) 5, doi:10.1016/j.physletb.2015.04.002, arXiv:1412.4109.
- [14] ATLAS Collaboration, "Search for supersymmetry at $\sqrt{s} = 13$ TeV in final states with jets and two same-sign leptons or three leptons with the ATLAS detector", *Eur. Phys. J. C* **76** (2016), no. 5, 259, doi:10.1140/epjc/s10052-016-4095-8, arXiv:1602.09058.
- [15] CMS Collaboration, "Search for SUSY with multileptons in 13 TeV data", (2016). arXiv:1701.06940. Submitted to *EPJC*.
- [16] CMS Collaboration, "The CMS experiment at the CERN LHC", *JINST* **3** (2008) S08004, doi:10.1088/1748-0221/3/08/S08004.

- [17] CMS Collaboration, “Particle-flow event reconstruction in CMS and performance for jets, taus, and E_T^{miss} ”, CMS Physics Analysis Summary CMS-PAS-PFT-09-001, CERN, 2009.
- [18] CMS Collaboration, “Commissioning of the particle-flow event reconstruction with the first LHC collisions recorded in the CMS detector”, CMS Physics Analysis Summary CMS-PAS-PFT-10-001, CERN, 2010.
- [19] CMS Collaboration, “Commissioning of the Particle-Flow Reconstruction in Minimum-Bias and Jet Events from pp Collisions at 7 TeV”, CMS Physics Analysis Summary CMS-PAS-PFT-10-002, 2010.
- [20] M. Cacciari, G. P. Salam, and G. Soyez, “The anti- k_t jet clustering algorithm”, *JHEP* **04** (2008) 063, doi:10.1088/1126-6708/2008/04/063, arXiv:0802.1189.
- [21] CMS Collaboration, “Identification of b-quark jets with the CMS experiment”, *JINST* **8** (2013) P04013, doi:10.1088/1748-0221/8/04/P04013, arXiv:1211.4462.
- [22] CMS Collaboration, “Performance of b tagging at $\sqrt{s}=8$ TeV in multijet, $t\bar{t}$ and boosted topology events”, CMS Physics Analysis Summary CMS-PAS-BTV-13-001, 2013.
- [23] CMS Collaboration, “Performance of CMS muon reconstruction in pp collision events at $\sqrt{s} = 7$ TeV”, *JINST* **7** (2012) P10002, doi:10.1088/1748-0221/7/10/P10002, arXiv:1206.4071.
- [24] CMS Collaboration, “Performance of Electron Reconstruction and Selection with the CMS Detector in Proton-Proton Collisions at $v_s = 8$ TeV”, *JINST* **10** (2015) P06005, doi:10.1088/1748-0221/10/06/P06005, arXiv:1502.02701.
- [25] CMS Collaboration, “Performance of the missing transverse energy reconstruction by the CMS experiment in $\sqrt{s} = 8$ TeV pp data”, (2014). arXiv:1411.0511. Submitted to *JINST*.
- [26] J. Alwall et al., “The automated computation of tree-level and next-to-leading order differential cross sections, and their matching to parton shower simulations”, *JHEP* **07** (2014) 079, doi:10.1007/JHEP07(2014)079, arXiv:1405.0301.
- [27] T. Melia, P. Nason, R. Rontsch, and G. Zanderighi, “W+W-, WZ and ZZ production in the POWHEG BOX”, *JHEP* **11** (2011) 078, doi:10.1007/JHEP11(2011)078, arXiv:1107.5051.
- [28] T. Sjostrand, S. Mrenna, and P. Z. Skands, “A Brief Introduction to PYTHIA 8.1”, *Comput. Phys. Commun.* **178** (2008) 852, doi:10.1016/j.cpc.2008.01.036, arXiv:0710.3820.
- [29] CMS Collaboration, “Event generator tunes obtained from underlying event and multiparton scattering measurements”, *Eur. Phys. J. C* **76** (2016) 155, doi:10.1140/epjc/s10052-016-3988-x, arXiv:1512.00815.
- [30] GEANT4 Collaboration, “GEANT4—a simulation toolkit”, *Nucl. Instrum. Meth. A* **506** (2003) 250, doi:10.1016/S0168-9002(03)01368-8.
- [31] S. Abdullin et al., “The fast simulation of the CMS detector at LHC”, *J. Phys. Conf. Ser.* **331** (2011) 032049, doi:10.1088/1742-6596/331/3/032049.

- [32] W. Beenakker et al., “Production of charginos, neutralinos, and sleptons at hadron colliders”, *Phys. Rev. Lett.* **83** (1999) 3780, doi:10.1103/PhysRevLett.83.3780, arXiv:hep-ph/9906298.
- [33] A. Kulesza and L. Motyka, “Threshold resummation for squark-antisquark and gluino-pair production at the LHC”, *Phys. Rev. Lett.* **102** (2009) 111802, doi:10.1103/PhysRevLett.102.111802, arXiv:0807.2405.
- [34] A. Kulesza and L. Motyka, “Soft gluon resummation for the production of gluino-gluino and squark-antisquark pairs at the LHC”, *Phys. Rev. D* **80** (2009) 095004, doi:10.1103/PhysRevD.80.095004, arXiv:0905.4749.
- [35] W. Beenakker et al., “Soft-gluon resummation for squark and gluino hadroproduction”, *JHEP* **12** (2009) 041, doi:10.1088/1126-6708/2009/12/041, arXiv:0909.4418.
- [36] W. Beenakker et al., “Squark and gluino hadroproduction”, *Int. J. Mod. Phys. A* **26** (2011) 2637, doi:10.1142/S0217751X11053560, arXiv:1105.1110.
- [37] J. Butterworth et al., “PDF4LHC recommendations for LHC Run II”, *J. Phys. G* **43** (2016) 023001, doi:10.1088/0954-3899/43/2/023001, arXiv:1510.03865.
- [38] T. Junk, “Confidence level computation for combining searches with small statistics”, *Nucl. Instrum. Meth. A* **434** (1999) 435, doi:10.1016/S0168-9002(99)00498-2, arXiv:hep-ex/9902006.
- [39] A. L. Read, “Presentation of search results: The CL_s technique”, *J. Phys. G* **28** (2002) 2693, doi:10.1088/0954-3899/28/10/313.
- [40] ATLAS and CMS Collaborations, “Procedure for the LHC Higgs boson search combination in summer 2011”, Technical Report ATL-PHYS-PUB-2011-11, CMS-NOTE-2011-005, CERN, 2011.